Mon. Not. R. Astron. Soc. **398,** 221–232 (2009) doi:10.1111/j.1365-2966.2009.14934.x

A study of the Galactic plane towards $l = 305°$

G. Baume,[1⋆]† G. Carraro[2⋆]‡ and Y. Momany[2⋆]§

[1]*Facultad de Ciencias Astronómicas y Geofísicas (UNLP), Instituto de Astrofísica de La Plata (CONICET, UNLP), Paseo del Bosque s/n, La Plata, Argentina*

[2]*ESO, Alonso de Cordova 3107, Vitacura, Santiago de Chile, Chile*

Accepted 2009 April 16. Received 2009 April 16; in original form 2009 March 6

ABSTRACT

We present optical ($UBVI_C$) observations of a rich and complex field in the Galactic plane towards $l \sim 305°$ and $b \sim 0°$. Our analysis reveals a significantly high interstellar absorption ($A_V \sim 10$) and an abnormal extinction law in this line of sight. Availing a considerable number of colour combinations, the photometric diagrams allow us to derive new estimates of the fundamental parameters of the two open clusters Danks 1 and Danks 2. Due to the derived abnormal reddening law in this line of sight, both clusters appear much closer (to the Sun) than previously thought. Additionally, we present the optical colours and magnitudes of the WR 48a star, and its main parameters were estimated. The properties of the two embedded clusters, DBS2003 130 and 131, are also addressed. We identify a number of young stellar objects which are probable members of these clusters. This new material is then used to revisit the spiral structure in this sector of the Galaxy showing evidence of populations associated with the inner Galaxy Scutum-Crux arm.

Key words: stars: individual: WR 48a – open clusters and associations: general – Galaxy: structure.

1 INTRODUCTION

The study of embedded Galactic clusters is fundamental in tracing the Galactic spiral structure and improves our understanding of the star formation process. Our group has investigated several Galactic plane regions in the fourth quadrant line of sights (see Vázquez et al. 2005; Carraro & Costa 2009), and in this paper we further extend this study to a region located at $l = 305°$ and $b \sim 0°$. This region contains very interesting objects: an important cloud which obscures two compact young open clusters (Danks 1 and Danks 2), a WR star (WR 48a) and at least three embedded clusters (DBS2003 130, 131 and 132) so far detected only in the infrared (IR) (Dutra et al. 2003). There are also several H II regions and OH/H_2O maser sources (see Danks et al. 1984 or Clark & Porter 2004 for a detailed description).

The open clusters Danks 1 and Danks 2 were first detected by Danks et al. (1983), and their parameters were only recently estimated by Bica et al. (2004), using *BVI* and *JHK* photometry. In this regard, we show that complementing the optical and IR data with *U* observations adds valuable information that allows a better determination of the interstellar absorption in this line of sight. As for the embedded clusters, it is important to note that only DBS2003 131 has been extensively studied in the IR (Leistra et al. 2005; Longmore et al. 2007), and that none of three clusters has been studied in the optical.

In this paper, we perform a detailed wide field study at $l = 305°$ using all *UBVI* and *JHK*, of all the aforementioned objects, and derive updated estimates of their fundamental parameters. We then analyse this field with respect to other fields in the fourth Galactic quadrant to derive information about the Galactic spiral structure of this portion of the disc.

The layout of this paper is as follows. In Section 2, we describe the used data, and the reduction and calibration procedures. In Section 3, we present the analysis of the data together with the main cluster parameters. Finally, in Sections 4 and 5 we discuss and summarize our results.

2 DATA

2.1 Observations

$UBVI_C$ images of the region under study (see Fig. 1) were acquired using the Y4KCAM camera attached to the 1.0-m telescope, which is operated by the Small and Moderate Aperture Research Telescope System (SMARTS) consortium[1] and placed at Cerro Tololo Inter-American Observatory (CTIO). This camera is equipped with a 4064 × 4064 CCD with 15 μ pixels. This setup provides direct imaging over a field of view (FOV) 20.0 × 20.0 arcmin^2 with a

⋆E-mail: gbaume@fcaglp.fcaglp.unlp.edu.ar (GB); gcarraro@eso.org (GC); ymomany@eso.org (YM)

†Member of Carrera del Investigador CONICET, Argentina.

‡On leave from Dipartimento di Astronomia, Università di Padova, Vicolo Osservatorio 2, I-35122, Padova, Italy.

§On leave from INAF, Osservatorio Astronomico di Padova, Vicolo Osservatorio 2, I-35122, Padova, Italy.

[1] http://www.astro.yale.edu/smarts

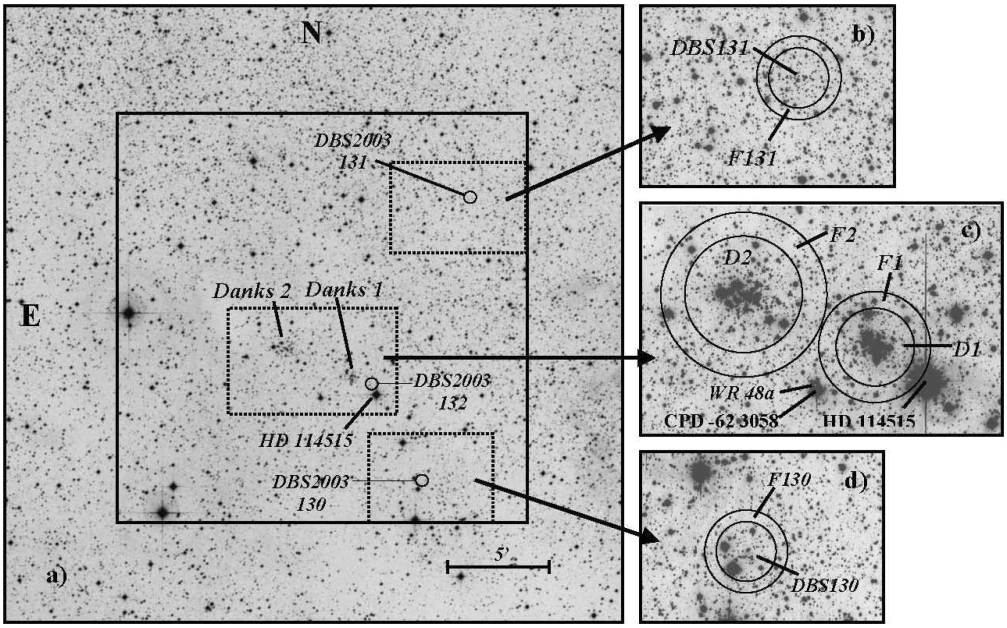

Figure 1. Left-hand image (panel a) shows a second generation DSS-2 (red filter) image centred at $\alpha_{2000} = 13{:}12{:}43.4$, $\delta_{2000} = -62{:}39{:}2.2$ and covering a field of 30.0×30.0 arcmin^2. Open clusters Danks 1/2; embedded clusters DBS2003 130, 131 and 132; and HD 1145115 star are identified. Solid square indicates the full studied area, whereas the dotted rectangles trace the regions highlighted in the right panels (b, c and d), as these appear on our long *I* exposure.

scale of 0.289 arcsec pixel^{-1}. The relatively large FOV allowed us to include several objects present in the region and also to have an important sample of the adjacent stellar field in this part of the Galactic plane. The CCD was operated without binning, at a nominal gain and read-out noise of 1.44 e-/ADU and 7 e- (this detector is read by means of four different amplifiers). Other detector characteristics can be found at http://www.astronomy.ohio-state.edu/Y4KCam/detector.html. Details on the observations are given in Table 1. Typical full width at half-maximum of the data was about 0.9 arcsec, and airmass values during the observation of the scientific frames ranged from 1.19 to 1.22.

2.2 Reduction

All frames were pre-processed in a standard way using the IRAF[2] package CCDRED. To this aim, zero exposures and sky flats were taken every night. In order to achieve deep photometry, all the long exposures within each band were combined using IMCOMBINE task. This procedure helps to remove cosmic rays and improve the signal-to-noise ratio of the faintest stars. In particular, five images were combined in *U* band, allowing us to reach the $U - B$ index for the brightest stars of Danks 1 and Danks 2. However, it was not enough for the case of embedded clusters, where only data in *BVI* bands could be obtained.

Photometry was then performed using IRAF DAOPHOT and PHOTCAL packages. Instrumental magnitudes were obtained using the point spread function (PSF) method (Stetson 1987). Since the FOV is large, a quadratic spatially variable PSF was adopted and its calibration on each image was done using several isolated, spatially well-distributed, bright stars (about 25) across the field. The PSF photometry was finally aperture-corrected for each filter and exposure time. Aperture corrections were computed performing aperture photometry of a suitable number (about 20) of bright stars in the field. In order to obtain a more complete sample of the stars in the observed region, an additional photometry table was generated using as input the coordinates (converted to pixels) of all the stars that according to the Two-Micron All-Sky Survey (2MASS) catalogue must be present in our FOV. Finally, all data from different filters and exposures were combined and calibrated using DAOMASTER (Stetson 1992).

[2] IRAF is distributed by National Optical Astronomy Observatory, which is operated by the Association of Universities for Research in Astronomy (AURA) under cooperative agreement with the National Science Foundation (NSF).

2.3 Photometric calibration

Standard star-selected areas (see Table 1) from the catalogue of Landolt (1992) were used to determine the transformation equations relating our instrumental magnitudes to the standard $UBVI_C$ system. The selection of the fields was done in order to provide a wide range in colours. Then, aperture photometry was carried out for all the standard stars (∼70 per night) using the IRAF PHOTCAL package. To tie our observations to the standard system, we use transformation equations of the form

$$u = U + u_1 + u_2(U - B) + u_3 X \qquad (\mathrm{rms} = 0.04) \qquad (1)$$

$$b = B + b_1 + b_2(B - V) + b_3 X \qquad (\mathrm{rms} = 0.03) \qquad (2)$$

$$v = V + v_{1bv} + v_{2bv}(B - V) + v_3 X \qquad (\mathrm{rms} = 0.02) \qquad (3)$$

$$v = V + v_{1vi} + v_{2vi}(V - I_C) + v_3 X \qquad (\mathrm{rms} = 0.02) \qquad (4)$$

$$i = I_C + i_1 + i_2(V - I_C) + i_3 X \qquad (\mathrm{rms} = 0.02), \qquad (5)$$

where $UBVI_C$ and *ubvi* are standard and instrumental magnitudes, respectively, and *X* is the airmass of the observation. The transformation coefficients and extinction coefficients for the CTIO Observatory are shown at the bottom of Table 1. To derive *V* magnitudes, we use expression (3) when the *B* magnitude was available; otherwise expression (4) was used.

Table 1. Journal of observations of the scientific frames together with used calibration coefficients (2006 March 23 and 24).

Exposure times (s) × N Date	Frames	U	B	V	I_C	N_f
Scientific frames						
23 and 24	Long	2000 × 5	1200 × 2	900 × 2	700 × 2	1
	Medium	200 × 2	100 × 2	100 × 2	100 × 2	1
	Short	30 × 2	30 × 2	30 × 2	30 × 2	1
Standard frames (Landolt 1992)						
23	SA101	400	200	150	130	2
	SA107	200	50	30	30	3
24	SA101	400	200	150	130	2
	SA101	200	50	30	30	1
	SA104	400	200	150	130	1
	SA104	200	50	30	30	1
	SA107	200	50	30	30	3
Calibration and extinction coefficients						
$u_1 = +3.284 \pm 0.007$			$v_{1bv} = +1.822 \pm 0.010$			
$u_2 = -0.025 \pm 0.012$			$v_{2bv} = -0.054 \pm 0.012$			
$u_3 = +0.45$			$v_{1vi} = +1.836 \pm 0.008$			
$b_1 = +2.025 \pm 0.012$			$v_{2vi} = -0.059 \pm 0.009$			
$b_2 = +0.167 \pm 0.015$			$v_3 = +0.16$			
$b_3 = +0.25$			$i_1 = +2.677 \pm 0.016$			
			$i_2 = -0.002 \pm 0.018$			
			$i_3 = +0.08$			

Note. N indicates the number of obtained exposures in case it is more than 1, while N_f indicates the amount of different observed frames in each field.

2.4 Complementary data and astrometry

Other available catalogues, such as the 2MASS (Cutri et al. 2003; Skrutskie et al. 2006), are of fundamental importance to perform a more complete analysis of the region under investigation. Therefore, using the *X*–*Y* stellar positions obtained from our data, their equatorial coordinates were computed. First of all, a matched list of *X*–*Y* and RA, Dec. was built by visually identifying about 20 2MASS stars in the field under study. The stars in the list were then used to obtain transformation equations to get equatorial coordinates for the remaining stars. In a second step, a computer routine was used to cross-identify all the sources in common with the same catalogues by matching the equatorial coordinates to the catalogued ones. The rms of the residuals was ∼0.17 arcsec, which is about the astrometric precision of the 2MASS catalogue (∼0.12 arcsec), as expected since most of the coordinates were retrieved from this catalogue.

2.5 Final catalogue

The above procedure allowed us to build an astrometric, photometric (*UBVIJHK*) catalogue that constitutes the main observational data base used in this study. A solid analysis of the behaviour of the stellar energy distributions can be carried out with this tool, thus preventing possible degeneracies in the photometric diagrams and allowing us to obtain more reliable results. The full catalogue with a total of 34 310 stars is only available in electronic form at the Centre de Donnes astronomiques de Strasbourg (CDS). It includes *X*–*Y* positions, 2MASS identification (when available), equatorial coordinates (epoch 2000.0), optical and 2MASS photometry. Table 2 is a summary of that catalogue including only stars adopted as likely cluster members or probable young stellar objects (YSOs).

3 DATA ANALYSIS

3.1 Selection of zones

With the aim of simplifying the analysis of the data, the studied region was divided into several sets presented in Table 3 (see also Fig. 1).

In this manner, $D1, D2$, $DBS130$ and $DBS131$ correspond to the regions involving the studied clusters and their surrounding areas; while $F1, F2$, $F130$ and $F131$ correspond to the respective, adopted, comparison field for each cluster. We emphasize on two facts: (a) each comparison field covers the same sky area as the corresponding cluster region and (b), as will be explained in Section 3.3.2, embedded cluster BDS2003 132 was not included in this study.

3.2 Photometric diagrams

The two-colour diagrams (TCDs) and colour–magnitude diagrams (CMDs) of the different zones are shown in Figs 2–10 in a self-explanatory format (see also Section 3.1).

The TCDs of the cluster zones (Figs 2, 4 and 7) clearly show the presence of the expected field population along with a heavily reddened ($E_{B-V} \sim 2.5$) group of stars, most likely cluster members. In all studied zones, $B - V$ versus $V - I$ diagrams confirm the above-mentioned trend and show that the cluster members suffer abnormal reddening laws, unlike the field population which follow a normal one. As a consequence, individual $R\,(= A_V/E_{B-V})$ values were derived for each cluster.

The optical CMDs of the cluster zones (Figs 3, 5 and 8) also illustrate that the cluster populations are made of very reddened stars. According to the IR CMDs, 2MASS data do not have enough precision to improve the information obtained from the optical

Table 2. A sample of the final catalogue used in this study.

ID	2MASS ID	X(pixel)	Y(pixel)	α_{J2000}	δ_{J2000}	V	$B-V$	$U-B$	$V-I$	K	$J-H$	$H-K$	Comments	
256	J13122855-6241438	1662.1	2563.4	13:12:28.6	−62:41:43.4	14.964	2.448	1.389	3.720	6.610	0.989	0.656	D1	lm
659	J13122850-6241509	1660.7	2587.8	13:12:28.5	−62:41:50.5	16.214	2.417	1.426	3.854	8.150	0.979	0.684	D1	lm
733	J13122626-6242095	1607.8	2652.7	13:12:26.3	−62:42:09.2	16.359	2.466	1.283	3.679	8.507	0.906	0.499	D1	lm
1124	J13122617-6241576	1605.9	2611.5	13:12:26.2	−62:41:57.3	16.954	2.744	1.349	4.028	7.756	1.294	0.560	D1	lm
1527	J13122369-6242013	1546.9	2623.8	13:12:23.8	−62:42:00.8	17.355	2.771	1.772	4.519	7.531	1.218	0.665	D1	lm
1578	J13122497-6242002	1576.7	2619.6	13:12:25.0	−62:41:59.6	17.401	2.622	1.819	4.520	7.477	1.276	0.669	D1	lm
2683	J13122678-6241571	1621.4	2607.2	13:12:26.9	−62:41:56.0	18.160	2.406	1.905	4.019	8.135	2.076	0.566	D1	lm
2819	J13123412-6241359	1793.8	2535.6	13:12:34.1	−62:41:35.4	18.228	2.108	1.296	3.551	10.798	0.878	0.418	D1	lm
2861	–	1650.6	2551.2	13:12:28.1	−62:41:39.9	18.251	2.219	1.140	3.559	–	–	–	D1	lm
3335	J13122721-6242041	1630.7	2633.8	13:12:27.3	−62:42:03.7	18.480	2.157	1.604	3.795	10.046	1.058	0.637	D1	lm
3505	–	1601.0	2609.4	13:12:26.0	−62:41:56.6	18.562	2.091	1.942	3.891	–	–	–	D1	lm
3518	–	1670.5	2579.6	13:12:28.9	−62:41:48.1	18.568	2.184	1.542	3.691	–	–	–	D1	lm
3694	J13122288-6241488	1527.4	2580.8	13:12:22.9	−62:41:48.4	18.644	2.256	1.818	4.196	9.644	1.057	0.571	D1	lm
3921	J13122693-6242147	1624.0	2669.3	13:12:27.0	−62:42:14.0	18.737	2.129	1.515	3.811	10.296	0.856	0.685	D1	lm
4046	–	1608.4	2605.5	13:12:26.3	−62:41:55.5	18.780	2.380	1.763	4.019	–	–	–	D1	lm
4122	J13122705-6242079	1626.3	2646.4	13:12:27.1	−62:42:07.3	18.806	2.098	1.350	3.544	9.770	0.861	1.888	D1	lm
4168	J13122525-6241555	1585.2	2605.3	13:12:25.4	−62:41:55.5	18.826	2.155	1.894	3.837	8.904	2.692	0.338	D1	lm
4502	J13122959-6241291	1685.7	2512.4	13:12:29.6	−62:41:28.7	18.938	2.112	1.950	3.683	11.069	0.944	0.458	D1	lm
4664	–	1610.3	2639.3	13:12:26.4	−62:42:05.3	18.990	2.106	1.486	3.587	–	–	–	D1	lm
5245	–	1624.6	2633.6	13:12:27.0	−62:42:03.7	19.207	2.293	1.917	3.682	–	–	–	D1	lm
5557	–	1602.8	2621.1	13:12:26.1	−62:42:00.0	19.304	2.333	1.723	3.848	–	–	–	D1	lm
5569	J13123061-6242081	1710.3	2647.6	13:12:30.6	−62:42:07.7	19.309	2.326	2.661	4.129	10.222	1.118	0.616	D1	lm
5833	J13122454-6242088	1565.7	2649.8	13:12:24.5	−62:42:08.3	19.391	2.136	2.106	4.089	10.433	1.103	0.565	D1	lm
6519	J13122498-6241456	1577.3	2568.3	13:12:25.0	−62:41:44.8	19.589	2.278	1.565	3.799	11.286	0.950	0.594	D1	lm
223	J13125643-6240283	2325.1	2300.8	13:12:56.4	−62:40:27.8	14.793	2.386	1.617	3.547	6.873	0.896	0.527	D2	lm
264	J13124634-6241262	2085.4	2501.7	13:12:46.3	−62:41:25.7	14.999	2.324	1.272	3.406	7.792	0.818	0.425	D2	lm
287	J13124958-6241207	2162.7	2482.7	13:12:49.6	−62:41:20.3	15.095	2.120	1.051	3.127	8.595	0.686	0.400	D2	lm
775	J13125627-6240515	2321.6	2381.5	13:12:56.2	−62:40:51.1	16.409	2.343	1.105	3.489	9.306	0.770	0.402	D2	lm
892	J13125456-6241050	2280.9	2428.3	13:12:54.5	−62:41:04.6	16.618	2.343	1.057	3.388	9.654	0.779	0.369	D2	lm
936	J13125236-6240463	2228.5	2363.6	13:12:52.3	−62:40:45.9	16.672	2.159	1.070	3.205	10.059	0.725	0.369	D2	lm
979	J13125864-6240552	2378.1	2394.4	13:12:58.6	−62:40:54.9	16.728	2.349	1.059	3.491	9.556	0.803	0.396	D2	lm
989	J13125396-6240475	2266.4	2367.6	13:12:53.9	−62:40:47.1	16.741	2.196	1.056	3.209	10.104	0.731	0.334	D2	lm
1026	J13125445-6240459	2278.0	2362.3	13:12:54.4	−62:40:45.5	16.795	2.273	0.907	3.291	9.920	0.802	0.416	D2	lm
1260	J13125829-6240371	2369.8	2331.4	13:12:58.3	−62:40:36.7	17.098	2.340	1.154	3.611	9.628	0.820	0.413	D2	lm
1409	J13125325-6240346	2249.7	2323.0	13:12:53.2	−62:40:34.2	17.247	2.076	0.945	3.343	10.529	0.735	0.342	D2	lm
1577	J13124747-6240547	2112.2	2392.4	13:12:47.5	−62:40:54.2	17.399	2.163	0.898	3.271	10.725	0.756	0.326	D2	lm
1608	J13125436-6240422	2276.1	2349.2	13:12:54.3	−62:40:41.8	17.428	2.219	1.080	3.354	10.529	0.763	0.359	D2	lm
1631	J13125731-6240268	2346.2	2296.5	13:12:57.3	−62:40:26.6	17.453	2.327	1.048	3.582	8.504	1.789	0.836	D2	lm
1671	J13125373-6240508	2261.3	2379.1	13:12:53.7	−62:40:50.4	17.489	2.230	1.017	3.376	10.477	0.779	0.363	D2	lm
1704	J13125356-6240119	2257.1	2243.9	13:12:53.6	−62:40:11.4	17.513	2.355	1.254	3.725	9.891	0.854	0.413	D2	lm
1792	J13125529-6240416	2297.7	2346.7	13:12:55.3	−62:40:41.0	17.580	2.382	0.840	3.302	10.307	0.745	0.439	D2	lm
2248	J13130084-6239545	2430.5	2183.7	13:13:00.8	−62:39:54.0	17.918	2.134	1.356	3.287	11.229	0.777	0.308	D2	lm

Table 2 – *continued*

ID	2MASS ID	X(pixel)	Y(pixel)	α_{J2000}	δ_{J2000}	V	$B-V$	$U-B$	$V-I$	K	$J-H$	$H-K$	Comments	
2272	J13125269-6240545	2236.6	2391.7	13:12:52.7	−62:40:54.0	17.931	2.132	1.014	3.217	11.293	0.728	0.309	D2	lm
2500	J13125226-6240242	2226.0	2286.5	13:12:52.2	−62:40:23.6	18.073	2.115	1.056	3.379	11.066	0.766	0.394	D2	lm
2533	J13125193-6240579	2218.5	2403.7	13:12:51.9	−62:40:57.5	18.091	2.110	1.165	3.377	11.107	0.784	0.373	D2	lm
2700	J13125237-6240314	2229.1	2311.9	13:12:52.4	−62:40:31.0	18.168	2.071	1.086	3.279	11.344	0.741	0.404	D2	lm
3215	J13124526-6240421	2059.3	2349.1	13:12:45.3	−62:40:41.7	18.426	2.042	2.545	3.291	11.079	1.139	0.376	D2	lm
3388	J13125828-6240526	2369.5	2385.1	13:12:58.3	−62:40:52.2	18.506	2.031	1.354	3.370	11.505	0.793	0.340	D2	lm
3199	J13115353-6246577	829.8	3652.4	13:11:53.6	−62:46:57.5	18.420	1.874	1.475	2.775	11.702	0.976	0.704	D130	yso?
3486	J13115601-6247114	889.3	3700.3	13:11:56.1	−62:47:11.4	18.554	2.062	3.299	2.974	11.787	1.035	0.473	D130	yso?
3624	J13115851-6247072	948.6	3685.4	13:11:58.6	−62:47:07.1	18.617	1.962	2.159	3.004	11.700	1.087	0.407	D130	yso?
9376	J13115519-6247072	870.8	3685.7	13:11:55.4	−62:47:07.2	20.249	2.111	2.696	3.310	12.308	1.392	−0.259	D130	yso?
12300	J13115237-6246517	801.3	3633.2	13:11:52.5	−62:46:52.0	20.720	2.146	0.021	2.607	13.956	1.009	1.021	D130	yso?
13396	–	774.4	3636.3	13:11:51.3	−62:46:52.9	20.889	1.991	1.244	2.669	–	–	–	D130	yso?
7046	–	439.8	785.8	13:11:37.4	−62:33:09.7	19.737	2.531	3.769	4.343	–	–	–	D131	yso?
9892	–	479.9	800.9	13:11:39.1	−62:33:14.1	20.337	3.125	1.362	5.469	–	–	–	D131	yso?
12192	–	406.2	798.5	13:11:36.0	−62:33:13.4	20.704	2.326	–	4.493	–	–	–	D131	yso?
13636	–	450.4	800.1	13:11:37.9	−62:33:13.8	20.924	6.467	–	3.997	–	–	–	D131	yso?
14868	J13114106-6232570	525.7	741.5	13:11:41.1	−62:32:57.0	21.107	2.553	−0.300	5.166	9.575	1.366	0.819	D131	yso?-A1
15897	–	520.6	741.9	13:11:40.8	−62:32:57.1	21.247	–	–	5.334	–	–	–	D131	yso?
16128	–	622.8	805.9	13:11:45.1	−62:33:15.6	21.277	2.664	1.699	5.888	–	–	–	D131	yso?
16664	–	347.5	847.0	13:11:33.6	−62:33:27.3	21.351	2.534	−0.207	5.002	–	–	–	D131	yso?-A2
18863	–	534.4	812.4	13:11:41.4	−62:33:17.4	21.632	2.821	0.596	4.837	–	–	–	D131	yso?-CO
21172	J13113947-6233283	487.9	850.0	13:11:39.5	−62:33:28.3	21.899	2.503	1.490	4.886	11.939	1.471	0.657	D131	yso?-A3
22042	–	417.2	791.1	13:11:36.5	−62:33:11.2	22.003	–	–	4.420	–	–	–	D131	yso?
25701	–	495.4	777.4	13:11:39.8	−62:33:07.3	22.452	2.685	0.942	4.791	–	–	–	D131	yso?
26479	–	496.5	818.1	13:11:39.8	−62:33:19.0	22.556	–	–	5.027	–	–	–	D131	yso?
28362	–	477.7	839.5	13:11:39.0	−62:33:25.2	22.873	2.629	–	5.341	–	–	–	D131	yso?
30644	J13113382-6233270	354.0	847.7	13:11:33.8	−62:33:27.5	23.475	–	–	3.694	10.342	1.308	0.678	D131	yso?

Note. Comments column indicates the star region location and its adopted membership (D1/2 = Danks 1/2 regions; D130/131 = DBS130/131 regions; lm = likely member; yso? = probable YSO; A1, A2, A3 and CO are identifications from Leistra et al. 2005).
A full version of this table is only available in electronic form at the CDS.

Table 3. Description of studied zones.

Name	Shape	Centre	Radius (r) (arcmin)
$D1$	Circle	Danks 1	0.96
$F1$	Corona	Danks 1	$0.96 < r < 1.36$
$D2$	Circle	Danks 2	1.44
$F2$	Corona	Danks 2	$1.44 < r < 2.04$
*DBS*130	Circle	DBS2003 130	0.72
$F130$	Corona	DBS2003 130	$0.72 < r < 1.02$
*DBS*131	Circle	DBS2003 131	0.72
$F131$	Corona	DBS2003 131	$0.72 < r < 1.02$
Field	The remaining observed area		

photometric diagrams. However, it is important to note that the chosen distance for each cluster (see Section 3.3) produced a coherent fit of the zero-age main sequence (ZAMS) or main sequence (MS) along all the CMDs (optical and IR) as lower envelopes of the adopted member stars.

3.3 Main objects in the studied region

3.3.1 Danks 1 and Danks 2

Danks 1 (C1309-624) and Danks 2 (C1310-624) are catalogued as open clusters with a diameter of 1.0 and 1.5 arcmin, respectively, and both classified with a Trumpler class 1-1-p- (Lyngå 1987; Dias et al. 2002). That is why the sizes of the respective regions ($D1$, $F1$, $D2$ and $F2$) were chosen (see Section 3.1) to analyse the cluster itself and the behaviour of its associated field, respectively. Although these clusters are more easily detectable in IR, still they appear as clear overdensities in Digitized Sky Survey 2 (DSS-2)

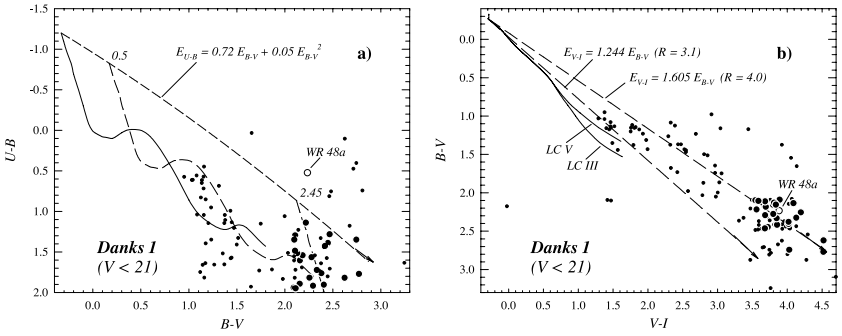

Figure 2. Optical TCDs of stars located in $D1$ zone. (see also Section 3.1 and Fig. 1 for zone definitions). (a) $U - B$ versus $B - V$ diagram. Heavy black circles are likely cluster members, whereas light dots are likely field stars. The solid line is the Schmidt-Kaler (1982) ZAMS, while dashed lines are the same ZAMS, but shifted along the reddening line by the adopted colour excesses indicated above them. They correspond to the adopted ones for the foreground population ($E_{B-V} = 0.5$) and for the cluster stars ($E_{B-V} = 2.45$) (see also Section 3.3). The dashed arrow indicates the normal reddening path. (b) $B - V$ versus $V - I$ diagrams. Symbols are the same as in panel (a) and solid lines are intrinsic colours for luminosity class V and III from Cousins (1978a,b). Dashed arrows indicate the reddening paths for normal ($R_V = 3.1$) and abnormal R_V values.

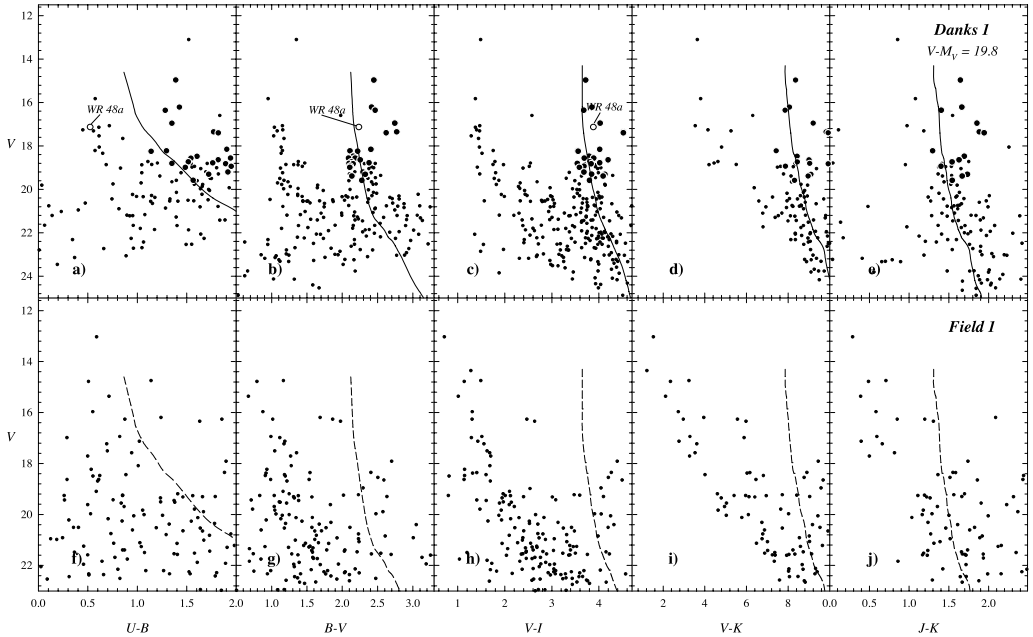

Figure 3. Optical CMDs of stars located in $D1$ and $F1$ zones (see also Section 3.1 and Fig. 1 for zone definitions). Symbols are the same as in Fig. 2. The solid and dashed curves are the Schmidt-Kaler (1982) empirical ZAMS and the MS path from Cousins (1978a,b) and Koornneef (1983). Solid curves are corrected by the adopted cluster apparent distance modulus (see Section 3.3).

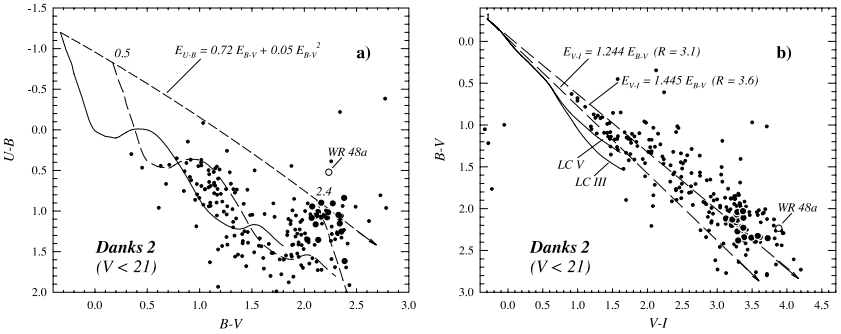

Figure 4. Optical TCDs of stars located in *D*2 zones (see also Section 3.1 and Fig. 1 for zone definitions). Symbols and curves are the same as in Fig. 2.

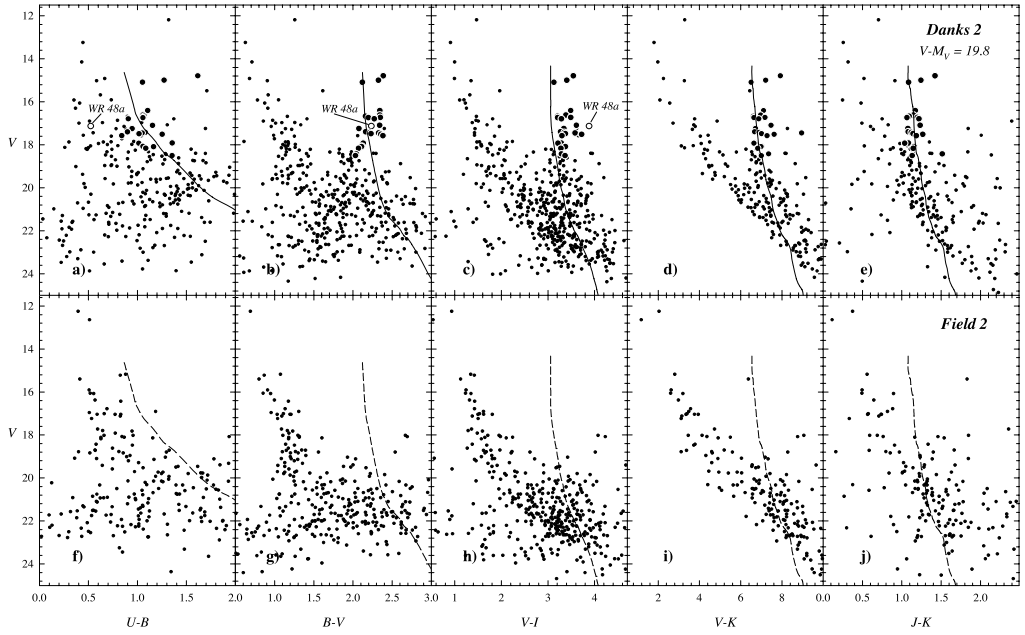

Figure 5. Optical CMDs of stars located in *D*2 and *F*2 zones (see also Section 3.1 and Fig. 1 for zone definitions). Symbols and curves are the same as in Fig. 3.

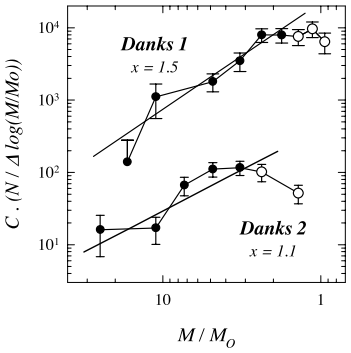

Figure 6. IMFs of Danks 1 (upper plot) and Danks 2 (lower plot). Error bars are from Poisson statistics. The least-square fittings for the more massive bins are indicated by solid right lines (open circles indicate bins not used in the fits. See the text for details). For clarity, each IMF was shifted by an arbitrary constant ('*C*').

(Fig. 1a). The adopted centres for the clusters were taken from SIMBAD and are presented in Table 4. Photometric diagrams of these clusters (Figs 2–5) show that they (i) suffer substantial reddening ($E_{B-V} = 2.45$ for Danks 1 and 2.4 for Danks 2), (ii) exhibit abnormal R value (3.6–4.0) and (iii) may also suffer a differential reddening across selected regions. In order to perform membership assignment, the individual position of the stars in all the photometric diagrams has been carefully inspected aiming at checking their consistency in all these diagrams simultaneously. This latter point was performed assuming that we were dealing with young populations, and the star positions on the CMDs were close to the location of a compatible ZAMS solution, by using previously adopted colour excess ratios and colour excess values. However, we allow for some dispersion around the adopted ZAMS due to the probable presence of dust inside the cluster, and also due to photometric errors (mainly in U band). As a following step, we took into account the number of stars for each magnitude bin according to the apparent luminosity functions (LFs) (see Baume et al. 2004a; Baume, Vázquez & Carraro 2004b; Baume et al. 2006). This procedure was applied for all stars down to an adopted $V_{\rm lim} \sim 19$. At fainter magnitudes, contamination by field stars becomes severe, preventing an easy identification of faint cluster members. The fit of a properly reddened Schmidt-Kaler (1982) ZAMS to the blue edge of the adopted member stars yields a distance modulus $V_0 - M_V = 10.0 \pm 0.3$ for Danks 1 and $V_0 - M_V = 11.5 \pm 0.3$ for Danks 2 (errors from eye inspection). An age of about 5 Myr can be estimated for both clusters taking into account the Meynet, Mermilliod & Maeder (1993) calibration. It must be noted that distance values are lower than

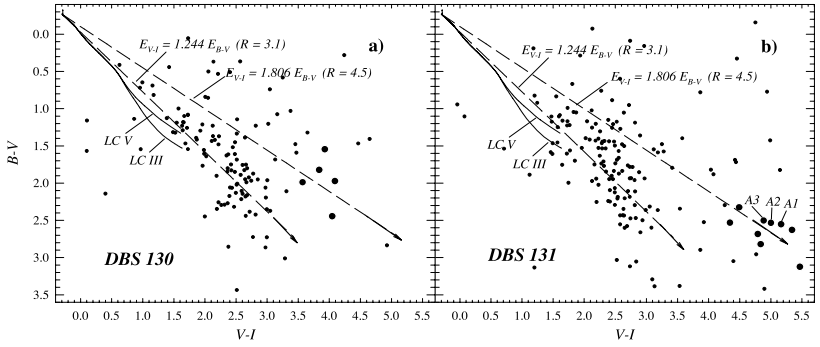

Figure 7. Optical TCDs of stars located in *DBS*130 and *DBS*131 zones (see also Section 3.1 and Fig. 1 for zone definitions). Symbols and curves are the same as in Fig. 2

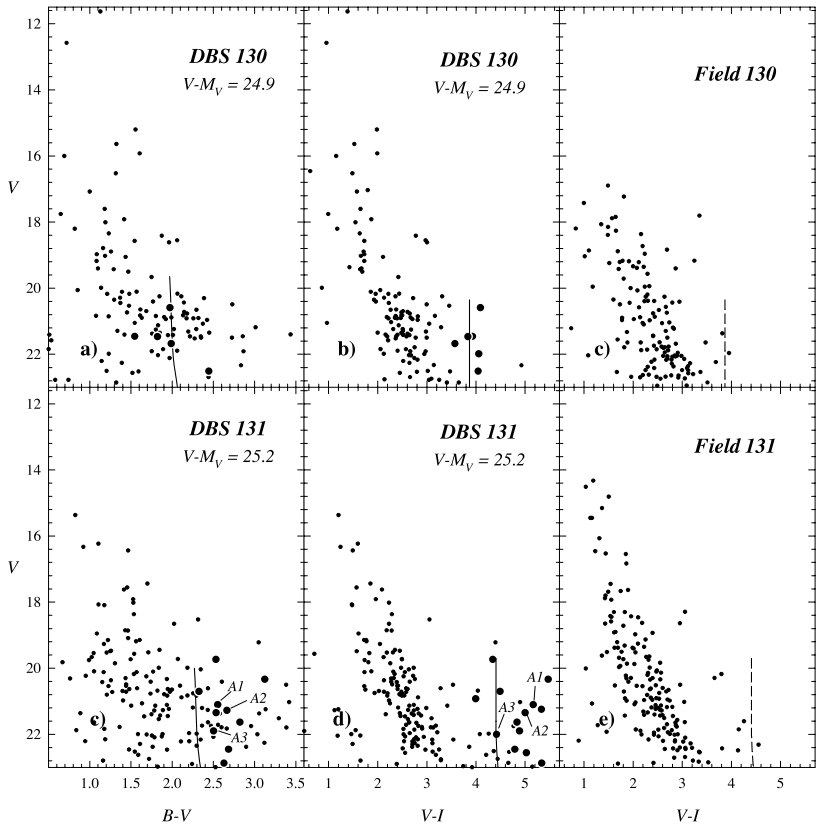

Figure 8. Optical CMDs of stars located in $DBS130, F130, DBS131$ and $F131$ zones (see also Section 3.1 and Fig. 1 for zone definitions). Symbols and curves are the same as in Fig. 3. $A1$, $A2$ and $A3$ are stars' identification from Leistra et al. (2005).

those obtained in previous works (e.g. Bica et al. 2004), and this is mainly due to the abnormal extinction law that we derive and adopt in this study.

To compute the cluster LFs and initial mass functions (IMFs), the following procedure was adopted.

(i) Stars located in cluster zones ($D1$ and $D2$) and comparison zones ($F1$ and $F2$) were selected. Additionally, in order to minimize the contamination of stars from the field population, only those stars with $V - I > (V - I)_{\rm lim}$ were considered [values of $(V - I)_{\rm lim}$ equal to 3.4 and 3.0 were adopted for $D1/F1$ and $D2/F2$, respectively]. All these stars were then called 'red stars'.

(ii) The apparent LFs of the clusters were obtained by subtracting the apparent LF of 'red stars' in the corresponding comparison zone ($F1$ or $F2$) from the apparent LF of 'red stars' placed in the clusters zones ($D1$ or $D2$). Bins were chosen in a way to avoid negative final values.

(iii) The resulting apparent LFs were shifted in magnitude to correct them by absorption and distance and to obtain the final LFs.

(iv) Finally, the IMFs of the clusters were computed by converting LF bins into mass bins using the mass–luminosity relation given by Scalo (1986).

The resulting apparent LFs and IMFs are presented in Table 5 and in Fig. 6, respectively, together with the corresponding IMF slopes.

3.3.2 *Embedded clusters*

The region under study contains three recently detected (Dutra et al. 2003), embedded clusters. They were identified as BDS2003 130,

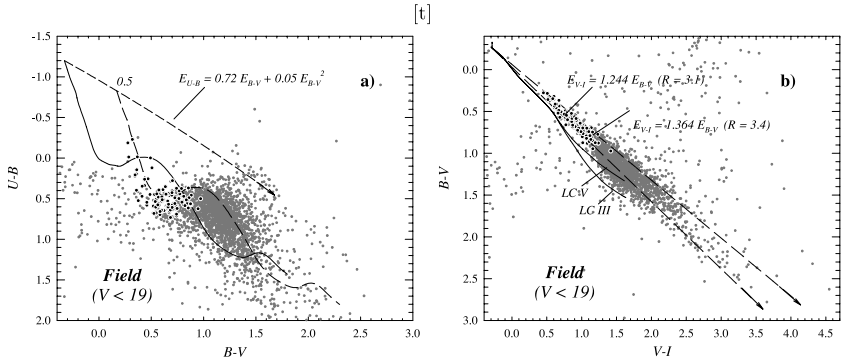

Figure 9. Optical TCDs of stars located in *Field* zone (see also Section 3.1 and Fig. 1 for zone definitions). Curves are the same as in Fig. 2.

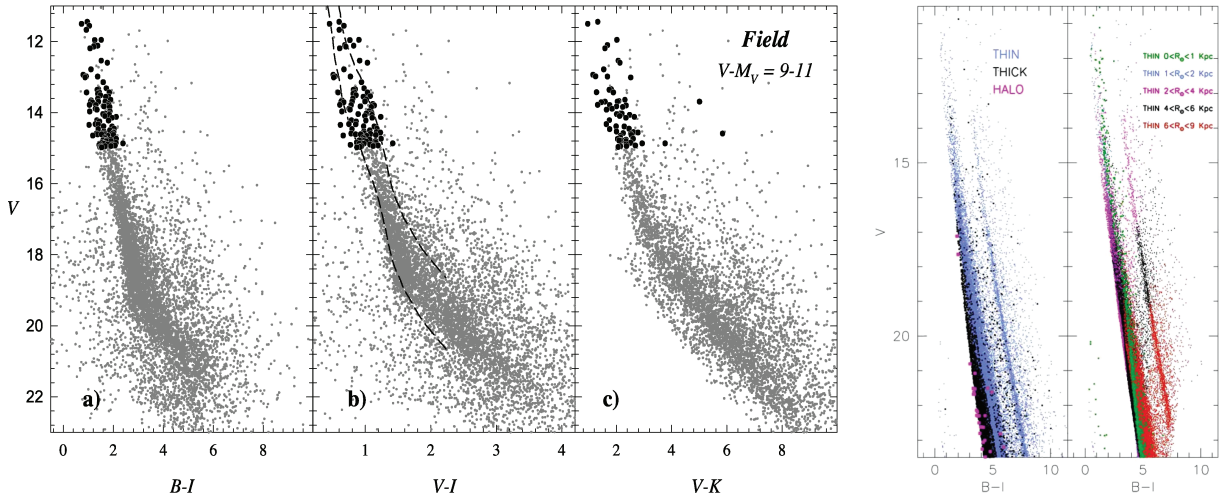

Figure 10. Left-hand plots: observational optical CMDs of stars located in *Field* zone (see Section 3.1 and Fig. 1 for zone definitions). Curves are the same as in Fig. 3. Right-hand plots: a simulation of the CMDs corresponding to the Galactic contribution along the $(l, b) = (305\overset{\circ}{.}37\ +0\overset{\circ}{.}12)$ line of sight. Left-hand panel highlights the different contribution of the thin/thick disc and halo populations. Right-hand panel shows the same simulation but analysing the distribution of the thin disc population at different distances along the line of sight. The red oblique sequence is best explained as due to the projection of giants and red clump stars at different distances.

Table 4. Parameters of the analysed stellar groups.

Stellar group	Centre		E_{B-V}	R	$V - M_V$	A_V	$V_0 - M_V$	Age (Myr)	IMF slope
	α_{2000}	δ_{2000}							
Danks 1	13:12:27.0	−62:41:59.7	2.45	4.0	19.80	9.8	10.0	∼5	∼1.5
Danks 2	13:12:55.3	−62:40:42.0	2.40	3.6	19.83	8.7	11.5	∼5	∼1.1
DBS2003 130	13:11:54.0	−62:47:02.0	2.3	∼4.5	∼24.9	10.4	14.5	∼1–3	–
DBS2003 131	13:11:39.4	−62:33:11.5	2.6	∼4.5	∼25.2	11.7	13.5	∼1–3	∼0.98–1.5
Foreground	13:12:43.4	−62:39:02.2	∼0.5	3.1	∼9–11	∼1.5	∼7.5–9.5	–	–

Note. Foreground coordinates correspond to the centre of the observed area (see Fig. 1).
IMF slope values for DBS2003 131 were taken from Leistra et al. (2005) and included for comparison.

131 and 132. Each cluster is, respectively, found very near to the H II regions G305.27−0.01, G305.3+0.2 and G305.3+0.1, which can also be identified, respectively, with the S155, S156 and S154 bubbles from the Churchwell et al. (2006) catalogue.

Our observations allowed us to obtain reliable information for BDS2003 130 and 131. Unfortunately, BDS2003 132 is too near to the position of star HD 114515 preventing detection of faint stars. Both BDS2003 130 and BDS2003 131 (=G305.3+0.2) are not visible in Fig. 1(a), and their presence is suggested only in our deep frames (see Figs 1b and d). Nevertheless, the CMDs of their zones (*DBS*130 and *DBS*131) clearly trace their presence, especially when the diagrams are compared with their respective comparison fields (*F*130 and *F*131) as shown in Fig. 8. Additionally, their TCDs (Fig. 7) reveal that both clusters suffer an abnormal extinction law and an $R \sim 4.5$ value is adopted for them. It must be noted that since almost all the considered cluster stars are at the limit of our photometry, their individual values must be taken as preliminary estimations and only the group structure in the diagrams can be considered valid. Still, stars indicated with black circles in the photometric diagrams can be considered as very probable YSOs.

In this way, it is possible to obtain an estimation of their parameters considering they are suffering a similar reddening than Danks

Table 5. Apparent LFs.

Danks 1		Danks 2	
ΔV	N	ΔV	N
14.0–16.0	1	14.0–16.0	3
16.0–18.0	4	16.0–17.0	6
18.0–19.0	13	17.0–18.0	12
19.0–20.0	12	18.0–19.0	20
20.0–21.0	22	19.0–20.0	20
21.0–22.0	20	20.0–22.0	14
22.0–23.0	16	22.0–24.0	12
23.0–24.0	17	24.0–26.0	0
24.0–25.0	10		

Table 6. Photometric data and adopted parameters for WR 48a.

Photometry		Parameters
U	19.89	$E_{B-V} \sim 2.4$
B	19.37	$R_{\rm ISM} \sim 3.8$
V	17.13	$(A_V)_{\rm ISM} \sim 9.1$
I	13.25	$(A_V)_{\rm CSM} \sim 2$
J	8.74	$V_0 - M_V \sim 10.9$
H	6.80	$M_V \sim -4.9$
K	5.09	

Note. JHK photometry was taken from the 2MASS catalogue.
M_V was taken from Lundström & Stenholm (1984).

1/2 ($E_{B-V} \sim 2.5$). This assumption is coherent with the $B - V$ values (∼2.1–2.4) of assumed YSO members. To estimate their distances, we again use a shifted Schmidt-Kaler (1982) ZAMS. The obtained cluster parameters are presented in Table 4. In the case of BDS2003 131, the distance is comparable with that derived in other studies (Leistra et al. 2005; Longmore et al. 2007) based on near-IR data or kinematic modelling of the related H II region (see Churchwell et al. 2006).

3.3.3 Star WR 48a

WR 48a is a WC9 star (Danks et al. 1983), and is placed within ∼1 arcmin of the clusters Danks 1/2. The distance estimation performed by Danks et al. (1983) was of 4 kpc; however van der Hucht (2001) concluded that it was only about 1.2 kpc away. On the other hand, the Danks et al. (1983) estimation of the absorption that this star is suffering is $A_V \sim 9.2$. This value is compatible with the values found for Danks 1/2 (see Table 4). Notwithstanding, the fact that WR stars can involve circumstellar envelopes producing intrinsic absorption seems reasonable to associate WR 48a star with the clusters Danks 1/2 distance. Given the photometric values obtained for this star (see Table 6) and its position in the CMDs of the clusters, its results are consistent with being a probable run away member as was previously assumed by Lundström & Stenholm (1984). In this case, the average values of the parameters between Danks 1/2 can be assumed for the WR star. In this way, the absorption value comes only from the interstellar medium (ISM) [$(A_V)_{\rm ISM}$] and adopting also $M_V = -4.9$ value from Lundström & Stenholm (1984) for a WC9 star, it is possible to estimate the circumstellar absorption [$(A_V)_{\rm CSM}$]. All the obtained values are presented in Table 6, and they indicate that only a minor amount of the total visual absorption is produced by the stellar envelope.

3.4 The field

The comparison of the photometric diagrams (TCDs and CMDs) of the field region is presented in Figs 9 and 10. The $U - B$ versus $B - V$ diagram reveals the presence of a relatively small group of blue stars (black symbols). On the other hand, all the CMDs show two clear parallel blue and red sequences.

For a deeper understanding of these diagrams, and in particular that of the parallel red sequence, we make a comparison between the observed diagrams and that of the expected Galactic contribution along this line of sight. The latter is estimated by making use of the Robin et al. (2003) Galactic model which provides synthetic CMDs at any given Galactic coordinates. These synthetic diagrams have been successfully used (e.g. Momany et al. 2004, 2006) to explain the presence of other seemingly anomalous features around Galactic open clusters. Fig. 10 (see the coloured version) compares the observed V versus $B - I$ CMD with the expected Galactic contribution along the $(l, b) = (305.^{\circ}37, +0.^{\circ}12)$ line of sight according to the Besançon simulation.[3] In the middle panel of the right-hand plot of Fig. 10, we first disentangle between the stellar populations belonging to the three simulated Galactic main components (thin and thick discs plus halo) in this direction. Clearly, the simulation shows that we expect little, if any, halo contribution, and that most of the Galactic contribution is due to thin disc populations. The true nature of the red and oblique sequence is best explained in the right-hand panel of the plot. Indeed, when analysing the distance distribution of the thin disc populations, the location of the red oblique sequence is re-constructed as the projection of red clump stars and bright giants at different distances.

Additionally, the use of the Schmidt-Kaler (1982) ZAMS indicates that the brighter part of the blue sequence (black symbols in the left-hand panel of Fig. 10) is associated with a nearby group of stars with $E_{B-V} \sim 0.5$ and a distance modulus $V - M_V \sim 9$–11, corresponding to about 350–750 pc.

4 DISCUSSION

4.1 The Galactic spiral structure in Carina and Centaurus regions

Previous investigations by our group (Vázquez et al. 2005; Carraro & Costa 2009) presented optical observations near the field addressed in this paper. The multiple young and blue populations along the line of view were found to reveal three different spiral features at increasing distance from the Sun.

In this paper, we strengthen this conclusion and lend further support to the presence of at least three populations in this Galactic sector: (i) the first is a spatially spread foreground population placed mainly between 350 and 750 pc; (ii) the second is situated just behind a very dark cloud at 1–3 kpc, and is represented by the clusters Danks 1/2, and finally (iii) a third population which is traced by the embedded clusters, located at about 5–7 kpc.

The results are illustrated in Fig. 11 where the Vallée (2005) spiral arms' model is also shown as dotted curves. In this plot, we summarized the recent findings of Carraro & Costa (2009), Vázquez et al. (2005) and this study. The various segments indicate the location and corresponding uncertainties of the different populations detected along the $l = 290^{\circ}, 305^{\circ}$ and 306° line of sight.

We confirmed the early findings by Vázquez et al. (2005) that the populations beyond the open cluster Stock 16 (their groups A

[3] Note that the synthetic diagrams do not suffer completeness effects.

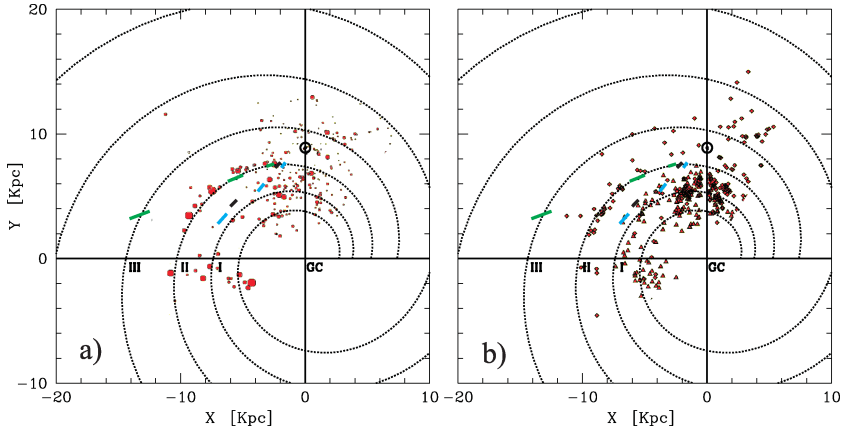

Figure 11. The groups we discuss in this paper are here superposed to the Vallée (2005) model of Galactic spiral structure (dotted curves) together with some of the H II regions (red symbols) adapted from Russeil (2003) in the left-hand panel (a) and from Paladini, Davies & DeZotti (2004) in the right-hand panel (b). Our groups are indicated as solid black segments representing their location and distance error. The green groups have been discussed in Carraro & Costa (2009) and are located at $l = 290^\circ$, whilst the blue groups have been studied by Vázquez et al. (2005) towards $l = 306^\circ$. The symbols I, II and III indicate the Scutum-Crux, Carina–Sagittarius and Perseus arms, respectively (see the text for more details).

and B) are most probably associated with Scutum-Crux. The same association could tentatively be done for the embedded clusters studied in this paper. The Danks 1/2 clusters, on the other hand, clearly belong to the Carina branch of the Carina–Sagittarius arm, like Stock 16 and the population A described in Carraro & Costa (2009). In this scenario it appears, however, that the Scutum-Crux arm as traced by Vallée should have a larger pitch angle than 11°. In fact, his plots indicate that this parameter has a $\sigma \approx 4^\circ$. However, some alternative scenarios are viable: (i) the observed displacement from the model can be accounted for by the natural width of 1 Kpc for spiral arms (see Vallée 2005) or (ii) the two most distant groups falling in between Scutum-Crux and Carina are tracing an inter-arm structure, or a branch of Carina. This latter possibility finds some support from the existence of several H II regions at the same position of these two groups (Russeil 2003; Paladini et al. 2004; see also Fig. 11).

More directions close to this region have to be studied. For example, more deeper, detailed and complementary analyses in different wavelengths as optical and IR by using objects as embedded clusters seem necessary to better trace the spiral structure in the fourth Galactic quadrant.

4.2 Cluster IMFs

There is an important spread in the IMF slopes computed for massive stars among several young clusters in the Galaxy. This is not yet fully understood, and can be attributed to the fact that (a) the IMF may not have a universal shape or/and (b) there are intrinsic mistakes in its computation (Scalo 1998).

Considering then the IMF slope given by

$$x = -\log(\mathrm{d}N/\mathrm{d}\log M)/\log M,$$

where dN is the number of stars within the logarithmic mass interval d log M around log M. The widely accepted slope values are $x = 1.35$ (Salpeter 1955) or 1.7 (Scalo 1998). However, in several very young open clusters (age $<10^7$ yr; see e.g. Baume et al. 2004a and references therein) we detect lower values for this parameter.

Our computed values for the clusters Danks 1/2 together with the value obtained by Leistra et al. (2005) for DBS2003 131 are presented in Table 4. The results are coherent and lie within the range of typically accepted values for very young clusters. However, we remark that our derived IMFs and their slope values are influenced by poor statistics.

5 CONCLUSIONS

A uniform and deep study was performed in a region of the Galactic plane towards $l = 305^\circ$. This region includes the open clusters Danks 1/2, their surrounding field and also three embedded IR clusters. The main properties of the different populations located along this line of sight were derived, and a description of ISM (through the colour excess behaviour) has allowed us to sketch a better picture of the observed clusters in this Galactic direction. In particular, the basic parameters of Danks 1/2, DBS2003 130 and 131, were determined. It must be noted that the method used, analysing each stellar photometric location and the inclusion of U filter, has helped us obtain mean distance values for the open clusters that are quite different from those derived in recent papers, where the latter are based on the analysis of only the global morphology of the CMDs. Additionally, our optical methods applied for classical embedded clusters offer compatible results with those specific ones used in IR, giving then more reliability to the results achieved in both cases. Our results indicate that in order to obtain better picture of complex and reddened regions, near-ultraviolet data are necessary. The performed analysis indicates that Danks 1/2 are almost at the same distance from the Sun, located probably on the Scutum-Crux arm. The analysis of the location of these grouping, together with previous detections in the same portion of the disc, is helping us to get a better picture of the spiral structure of the inner Milky Way.

Additionally, rough estimates of the IMFs for both objects were computed for the first time. The derived slope values were similar to those of other studied, addressing young open clusters. Lastly, the optical photometric values of WR 48a were presented and its main parameters were estimated, considering it as a runaway member of Danks 1/2.

ACKNOWLEDGMENTS

GB acknowledges support from CONICET (PIP 5970) and the staff of CTIO during all the run of the observations performed in 2006 March. The authors are much obliged for the use of the NASA Astrophysics Data System, SIMBAD data base (Centre de Donnés

Stellaires – Strasbourg, France) and WEBDA open cluster data base. This publication also made use of data from the 2MASS, which is a joint project of the University of Massachusetts and the Infrared Processing and Analysis Center/California Institute of Technology, funded by the National Aeronautics and Space Administration and the National Science Foundation.

REFERENCES

Baume G., Moitinho A., Giorgi E. E., Carraro G., Vázquez R. A., 2004a, A&A, 417, 961
Baume G., Vázquez R. A., Carraro G., 2004b, MNRAS, 355, 475
Baume G., Moitinho A., Vázquez R. A., Solivella G., Carraro G., Vilanova S., 2006, MNRAS, 367, 1441
Bica E., Ortolani S., Momany Y., Dutra C. M., Barbuy B., 2004, MNRAS, 352, 226
Carraro G., Costa E., 2009, A&A, 493, 71
Churchwell E. et al., 2006, ApJ, 649, 759
Clark J. S., Porter J. M., 2004, A&A, 427, 839
Cousins A. W. J., 1978a, Mon. Notes Astron. Soc. South. Afr., 37, 62
Cousins A. W. J., 1978b, Mon. Notes Astron. Soc. South. Afr., 37, 77
Cutri R. M. et al., 2003, University of Massachusetts and Infrared Processing and Analysis Center, California Institute of Technology
Danks A. C., Dennefeld M., Wamsteker W., Shaver P. A., 1983, A&A, 118, 301
Danks A. C., Wamsteker W., Shaver P. A., Retallack D. S., 1984, A&A, 132, 301
Dias W. S., Alessi B. S., Moitinho A., Lépine J. R. D., 2002, A&A, 389, 871
Dutra C. M., Bica E., Soares J., Barbuy B., 2003, A&A, 400, 533
Girardi L., Bressan A., Bertelli G., Chiosi C., 2000, A&AS, 141, 371
Koornneef J., 1983, A&A, 128, 84
Landolt A. U., 1992, AJ, 104, 340
Leistra A., Cotera A. S., Liebert J., Burton M., 2005, AJ, 130, 1719
Longmore S. N., Maercker M., Ramstedt S., Burton M. G., 2007, MNRAS, 380, 1497
Lundström I., Stenholm B., 1984, A&AS, 58, 163
Lyngå G., 1987, Catalog of Open Star Cluster Data. CDS, Strasbourg
Meynet G., Mermilliod J.-C., Maeder A., 1993, A&AS, 98, 477
Momany Y., Zaggia S. R., Bonifacio P., Piotto G., De Angeli F., Bedin L. R., Carraro G., 2004, A&A, 421, L29
Momany Y., Zaggia S., Gilmore G., Piotto G., Carraro G., Bedin L R., de Angeli F., 2006, A&A, 451, 515
Paladini R., Davies R. D., DeZotti G., 2004, MNRAS, 347, 237
Robin A. C., Reylé C., Derrière S., Picaud S., 2003, A&A, 409, 523
Russeil D., 2003, A&A, 397, 133
Salpeter E. E., 1955, ApJ, 121, 161
Scalo J., 1986, Fund. Cos. Phys., 11, 1
Scalo J., 1998, in Gilmore G., Howell D., eds, ASP Conf. Ser. Vol. 142, The Stellar Initial Mass Function: 38th Herstmonceux Conference. Astron. Soc. Pac., San Francisco, p. 201
Schmidt-Kaler Th., 1982, in Schaifers K., Voigt H. H., eds, Landolt-Börnstein, Numerical Data and Functional Relationships in Science and Technology, New Series, Group VI, Vol. 2(b), Springer Verlag, Berlin, p. 14
Skrutskie M. F. et al., 2006, AJ, 131, 1163
Stetson P. B., 1987, PASP, 99, 191
Stetson P. B., 1992, in Bulter C. J., Elliot I., eds, Proc. IAU Colloq. 136, Stellar Photometry-Current Techniques and Future Developments. Cambridge Univ. Press, Cambridge, p. 291
van der Hucht K. A., 2001, New Astron. Rev., 45, 135
Vallée J. P., 2005, AJ, 130, 569
Vázquez R. A., Baume G., Feinstein C., Nuñez J. A., Vergne M. M., 2005, A&A, 435, 883

This paper has been typeset from a TEX/LATEX file prepared by the author.